In Situ Scanning Tunneling Microscopy of Well-Defined Ir(111) Surface: High-Resolution Imaging of Adsorbed Sulfate

ARTICLE *in* THE JOURNAL OF PHYSICAL CHEMISTRY B · AUGUST 1999

Impact Factor: 3.3 · DOI: 10.1021/jp991112j

4 AUTHORS, INCLUDING:

Junji Inukai
University of Yamanashi
100 PUBLICATIONS **1,725** CITATIONS
SEE PROFILE

Kingo Itaya
Tohoku University
246 PUBLICATIONS **8,355** CITATIONS
SEE PROFILE

In Situ Scanning Tunneling Microscopy of Well-Defined Ir(111) Surface: High-Resolution Imaging of Adsorbed Sulfate

Li-Jun Wan, Masanori Hara, Jungi Inukai, and Kingo Itaya*

Department of Applied Chemistry, Graduate School of Engineering, Tohoku University, Aoba-yama 04, Sendai 980-8579, Japan

Received: April 1, 1999; In Final Form: June 14, 1999

It is demonstrated by using in situ scanning tunneling microscopy (STM) that well-defined Ir(111) surfaces can be exposed in aqueous solutions by a flame-annealing−quenching technique. Atomically flat terrace-step structures were consistently observed in the double layer potential range in an aqueous $HClO_4$ solution. It is shown that sulfate/bisulfate anions form highly ordered adlayers on Ir(111) in H_2SO_4 solution over a wide potential range. In situ STM images disclosed an Ir(111)−($\sqrt{3} \times \sqrt{7}$) structure, which is identical with that found previously on Au(111), Pt(111), Rh(111), and Cu(111). High-resolution STM imaging allowed us to determine the orientation of hydrogen-bonded water molecules. Two different water molecules were clearly distinguished as separate spots along the $\sqrt{3}$ direction between neighboring rows of adsorbed sulfate.

Introduction

The adsorption of sulfate/bisulfate has become an important issue in electrochemistry of well-defined surfaces,[1,2] since Clavilier and co-workers reported anomalous voltammograms on well-defined Pt(111) in sulfuric and perchloric acid solutions.[3−5] Although the anomalous state of adsorption observed on Pt(111) in sulfuric acid had long been interpreted as being due to the adsorption−desorption process of hydrogen,[5,6] the recent result reported by Clavilier and co-workers using a CO replacement technique indicated that the so-called butterfly peak observed on Pt(111) in sulfuric acid solution is probably due to the adsorption−desorption of sulfate/bisulfate rather than that of hydrogen.[7]

It has been demonstrated by several groups of investigators that in situ scanning tunneling microscopy (STM) can be used to visualize adsorbed sulfate/bisulfate (designated below simply as sulfate) species on Au(111),[8,9] Pt(111),[10,11] Rh(111),[12] and Cu(111).[13−15] An ordered structure with ($\sqrt{3} \times \sqrt{7}$) symmetry was first observed for the adsorbed sulfate on Au(111) in sulfuric acid by Magnussen et al.,[8] who proposed a model structure based on the assumption that the adsorbed species is bisulfate, not sulfate, with a surface coverage of 0.4. More recently, Weaver and co-workers also published STM images with the same symmetry of ($\sqrt{3} \times \sqrt{7}$) on Au(111),[9] but they proposed a possibility of incorporation of hydronium cations in the ordered sulfate adlayer based on the result that the surface coverage of sulfate on Au(111) determined by chronocoulometry and radiochemical assay is 0.2,[16] which is half the value proposed by Magnussen et al.

On Pt(111) surface, Stimming and co-workers found by in situ STM that adsorbed sulfate ions form the same ($\sqrt{3} \times \sqrt{7}$) adlayer structure as that found on Au(111).[10,11] Ordered domains with ($\sqrt{3} \times \sqrt{7}$) symmetry appeared in the potential range between 0.5 and 0.7 V vs a reversible hydrogen electrode (RHE) in 0.05 M H_2SO_4. Their STM observations confirmed that the butterfly peaks in sulfuric acid solutions are due to the adsorption−desorption of sulfate anions as shown by Clavilier using the CO replacement technique as described above.[7] The adlayer structure observed on Pt(111) was interpreted in terms of the coadsorption of sulfate anions and water molecules, which has previously been proposed by us for the adsorbed sulfate on Rh(111).[12]

The voltammetric behavior of Rh(111) in solutions containing sulfuric acid is very different from that of Pt(111) as first reported by Wieckowski's group.[17−19] The adsorption of sulfate seems to occur more strongly on Rh(111) than on Pt(111), because the hydrogen adsorption−desorption peaks on Rh(111) are strongly shifted toward negative potentials near the onset of the hydrogen evolution reaction in solutions containing sulfate.[12,18] The adlayer structure of sulfate on Rh(111) in sulfuric acid solution was revealed by in situ STM, as reported in our previous paper.[12] The ordered structure on Rh(111) is almost identical with that observed on Au(111) and Pt(111). We proposed a model structure to explain the nonuniform spacing in the unit cell of ($\sqrt{3} \times \sqrt{7}$), taking into account the existence of coadsorbed water molecules.[12] According to the coverage value of ca. 0.2 obtained on Rh(111) by Zelenay and Wieckowski,[20] hydrogen-bonded water chains are assumed to exist along the $\sqrt{3}$ direction between neighboring rows of adsorbed sulfate. Bright and dark spots appearing in the STM image were assumed to arise from adsorbed sulfate species and water molecules in the second layer of the first water bilayer.[12]

More recently, the adsorption of sulfate was investigated on Cu(111) surface in sulfuric acid by Wandelt's and Nichols's groups.[13−15] They have observed an ordered sulfate structure with the same ($\sqrt{3} \times \sqrt{7}$) symmetry as that observed on Au(111), Pt(111), and Rh(111) in H_2SO_4. The adlayer was proposed to be located on a reconstructed first Cu(111) layer, resulting in a distinct Moiré pattern in STM images. A mismatch of the first layer with the second layer of Cu substrate was suggested to be the origin of the Moiré pattern.[13−15]

Although it was expected to distinguish two different water molecules along the $\sqrt{3}$ direction according to our proposed model,[12] only one satellite spot was found in the unit cell of the ($\sqrt{3} \times \sqrt{7}$) structure on Au(111),[8,9] Pt(111),[10,11] and Rh(111).[12] However, Wandelt's group reported two satellite spots between the closely packed sulfate rows on Cu(111).[14]

In view of the previous studies mentioned above, the Ir(111) surface seems to be an interesting substrate for investigating

10.1021/jp991112j CCC: $18.00
Published on Web 08/03/1999

the adlayer of sulfate. Motoo and Furuya first reported characteristic peaks for the hydrogen adsorption−desorption reaction on Ir single-crystal surfaces.[21−23] More recently, Weaver's group investigated adsorbed nitric oxide and carbon monoxide on single crystals of Ir by using infrared absorption spectroscopy.[24−28] The electrochemical reduction of carbon dioxide was also investigated using Ir single-crystal electrodes.[29]

In the present paper, we, for the first time, report in situ electrochemical STM results of sulfate adsorption on well-defined Ir(111). Using a flame-annealing−quenching technique, we prepared an atomically flat Ir(111) surface. The Ir(111) surface and the sulfate adlayer in aqueous solution were intensively investigated by using in situ STM. The Ir(111)−(1 × 1) structure was consistently observed on terraces of Ir(111) in the double-layer potential region in $HClO_4$ solution, indicating that oxide-free, clean and unreconstructed surfaces exist in solution. The same ($\sqrt{3} \times \sqrt{7}$) sulfate structure was observed on the Ir(111) surface in 0.1 M H_2SO_4. Surprisingly, zigzag rows of hydrogen-bonded water molecules between neighboring sulfate rows along the $\sqrt{3}$ direction were clearly revealed. This observation further supports the proposed model of sulfate coadsorption with hydrogen-bonded water molecules described previously for the sulfate adlayer on Rh(111) surface.[12]

Experimental Section

Single-crystal Ir beads were made by the crystallization of a molten ball formed at one end of pure Ir wire (0.8 mm in diameter) in a hydrogen−oxygen flame. Well-prepared single-crystal beads showed eight facets of (111) in an octahedral configuration as described in the previous paper.[12] One of the facets was directly used for in situ STM observation. A laser-beam diffraction method was employed to determine the orientation of a so-prepared single-crystal bead to expose the (111) surface, which was then mechanically polished with successively finer grades of diamond paste down to 0.05 μm. The mechanically polished electrode was used to measure cyclic voltammograms (CVs) of Ir(111) in aqueous electrolyte solutions.

To expose an ordered and clean Ir(111) surface, the final treatment is extremely important. The flame-annealing−quenching technique was used in the present experiment. The Ir single crystal was annealed in a hydrogen−oxygen flame at about 2000 °C for 1 min and quickly brought into a hydrogen stream for a few seconds, and then immersed into ultrapure water saturated with hydrogen. The electrode was transferred into an electrochemical cell with a droplet of ultrapure water to protect the surface from contamination. It was ascertained by STM that the present procedure produces an atomically flat and clean Ir(111) surface with a (1 × 1) structure. Annealing at temperatures below ca. 1500 °C did not produce atomically flat surfaces, as described later.

All electrolyte solutions were prepared with ultrapure $HClO_4$ and H_2SO_4 from Cica-Merck and ultrapure water (Millipore-Q). All electrochemical potentials are reported with respect to RHE in the same electrolyte of 0.1 M $HClO_4$ or 0.1 M H_2SO_4.

The in situ STM imaging was performed with a Nanoscope E (Digital Instruments, Santa Barbara, CA), which was used with a modified STM electrochemical cell made from poly(chlorotrifluoroethylene). The tunneling tip was a tungsten wire with a diameter of 0.25 mm electrochemically etched in 0.6 M KOH by applying 12−15 V ac against a platinum electrode. The tips were partially coated with transparent nail polish to minimize the faradaic current. All STM images shown here were taken in the constant-current mode to evaluate corrugation heights of adsorbates and Ir substrate. Details of the STM experiment were identical with those described in our previous paper.[2,12]

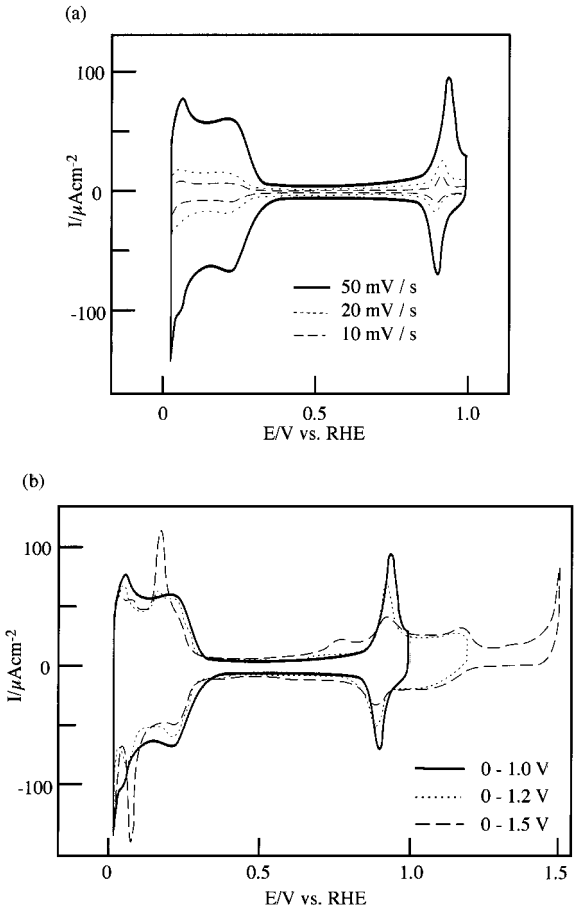

Figure 1. (a) Cyclic voltammograms of a well-defined Ir(111) electrode in 0.1 M $HClO_4$. The potential scan rate was 50, 20, and 10 mV/s as indicated. (b) Cyclic voltammograms obtained in a window-opening experiment in which the positive limit of the potential scan was varied. The potential scan rate was 50 mV/s.

Results and Discussion

Voltammetry. An Ir(111) electrode prepared by the flame-annealing−quenching method was transferred into 0.1 M $HClO_4$ or 0.1 M H_2SO_4 for CV measurements. By using a hanging meniscus method, only Ir(111) surface was exposed to the electrolyte solutions. Figure 1a shows a set of voltammograms obtained in 0.1 M $HClO_4$ at different scan rates in the potential range between 0.05 and 1.0 V. It can be seen that a double layer region extends from 0.35 to ca. 0.8 V. The hydrogen adsorption−desorption reaction appears between 0.05 and 0.35 V. Additional peaks can be seen at ca. 0.9 V. The peaks observed in the potential region shown in Figure 1a were found to be proportional to the scan rate. Overall features of the CVs are essentially the same as the previous results.[22,28,29] The charge involved in the hydrogen adsorption−desorption region was ca. 250 μC/cm^2. The number of atoms on the ideal Ir(111)−(1 × 1) surface is calculated to be 1.57×10^{15}/cm^2, which corresponds to the charge of 252 μC/ cm^2, assuming the formation of a hydrogen adlayer with a 1:1 ratio of H to Ir atoms involving a one-electron-transfer reaction. The charge found in this study suggests that the formation of a monolayer of hydrogen is completed before the hydrogen evolution reaction.

On the other hand, a pair of asymmetric peaks appeared at 0.95 V in the anodic scan and at 0.92 V in the cathodic scan,

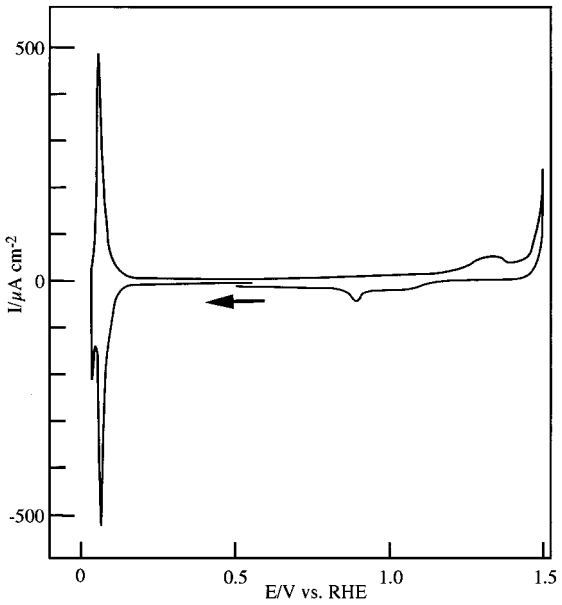

Figure 2. Cyclic voltammogram of a well-defined Ir(111) electrode in 0.1 M H_2SO_4. The potential scan rate was 50 mV/s.

respectively. Charge densities of approximately 100 μC/cm^2 were measured for those peaks. It is well-known that similar butterfly peaks appear on Pt(111) and Rh(111).[2,12,17] The peaks are probably due to the initial stages of surface oxidation, possibly the adsorption and desorption of hydroxide ions.

Figure 1b shows CVs obtained in a window-opening experiment, in which the positive limit of the potential scan was changed. When the voltammetric scan was extended to 1.2 V, the peaks at 0.9 V became broad and poorly defined. In the hydrogen adsorption−desorption region, a pair of asymmetric peaks appeared at 0.18 and 0.1 V in anodic and cathodic directions, respectively. The change in voltammetric feature became more pronounced when the upper limit was set at 1.5 V, where oxygen evolution commenced. This strongly suggests that the well-defined Ir(111) surface was roughened by the potential cycle with a limit more positive than 1.0 V.

Figure 2 shows a CV of Ir(111) in 0.1 M H_2SO_4. The electrode potential was first scanned in the negative direction from 0.55 V and reversed at a potential near the hydrogen evolution reaction. A small anodic peak was observed at 1.3 V before the oxygen evolution reaction, which seems to be due to the surface oxidation of the Ir(111) surface. An almost identical voltammogram was previously reported by Motoo and Furuya.[21,22] However, it is noteworthy that the characteristic sharp peaks seen in Figure 2 were unchanged in shape and height by several potential cycles between 0.05 and 1.0 V, suggesting that no surface roughening took place in this potential range. On the other hand, when the potential scan was reversed at 1.5 V, the peak height gradually decreased. This change in CV indicates that disordered Ir(111) surfaces appeared after the oxidation−reduction cycles of the well-defined Ir(111) surface even in H_2SO_4. It is also notable that the characteristic peaks observed in $HClO_4$ as shown in Figure 1a are now absent. The sharp cathodic peak appearing at 0.06 V in the sulfuric acid solution can be interpreted in terms of the displacement of adsorbed sulfate by hydrogen. The charge involved in the sharp peak was ca. 260 μC/cm^2, which is essentially equal to the value described in the previous paper.[21] A similar sharp peak was observed for Rh(111) in a sulfuric acid solution as described in our previous paper.[12] The dramatic change in the CV clearly indicates that sulfate ions are strongly adsorbed on the Ir(111) surface.

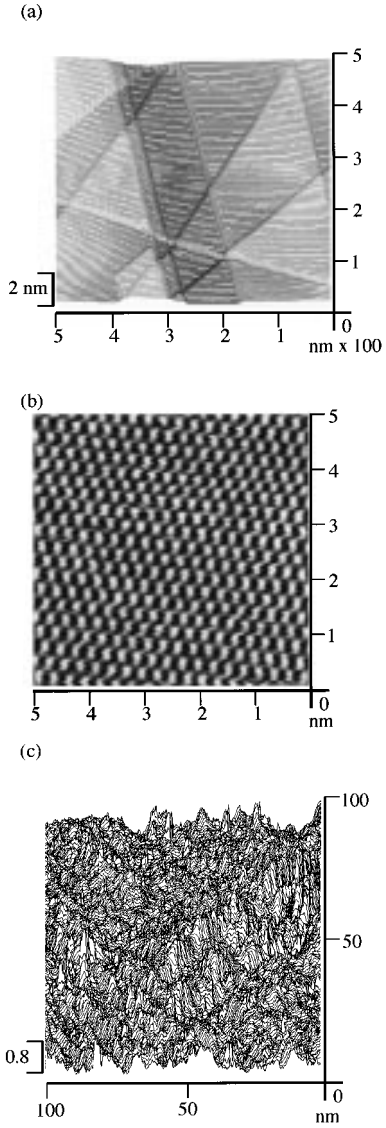

Figure 3. (a) STM topographic line scans observed on Ir(111) at 0.5 V in 0.1 M $HClO_4$. Tunneling current, 5 nA; tip potential, 0.55 V. (b) High-resolution STM image showing an Ir(111)−(1 × 1) structure. Tunneling current, 15 nA. (c) Topographic line scans observed on Ir(111) annealed at 1000 °C. Tunneling current, 5 nA.

In Situ STM in $HClO_4$. In situ STM was exclusively used to find appropriate conditions for the flame-annealing−quenching method employed to expose well-defined Ir(111) surfaces in solution. Figure 3a shows a typical large-scale STM image acquired in an area of 500 × 500 nm. This image was obtained at 0.5 V in 0.1 M $HClO_4$. Atomically flat surfaces with several monatomic step lines can be seen in this line plot image. The orientation of the monatomic steps differs by roughly 60° or 120° as expected for an fcc (111) surface with 3-fold symmetry.

The appearance of wide atomically flat terraces as can be seen in Figure 3a clearly shows that the flame-annealing−quenching technique produces well-defined Ir(111) surfaces. This image is the first direct evidence showing the existence of well-defined surfaces of Ir(111) in solution. The present study also revealed the atomic structure shown in Figure 3b, which was acquired in 0.1 M $HClO_4$ at the same electrode potential of 0.5 V as in Figure 3a. The tunneling current was changed in the range of 10−30 nA. A hexagonal structure can be seen under the present conditions with a nearest-neighbor spacing of 0.27 nm, indicating that the Ir(111) surface has a (1 × 1) structure. Identical atomic images were consistently observed in the

potential region between 0.1 and 1.0 V. We have focused our attention particularly on understanding the peaks at 0.9 V. After achieving atomic resolution at 0.5 V, as shown in Figure 3b, the electrode potential was scanned from 0.5 to 1.0 V in increments of 10 mV. However, no additional corrugation was found in STM images. The consistent appearance of Ir(111)−(1 × 1) structure suggests that the chemical species such as hydroxide involved in the peaks at 0.9 V might be mobile on the surface within the time scale of the STM measurement. The result described above is very similar to that observed on Rh(111) in 0.1 M $HClO_4$, in which the Rh(111)−(1 × 1) structure was consistently observed even at the positive potentials of the butterfly peak.[12]

STM investigations were made to observe the effect of annealing temperature on the surface structure. A roughened surface, as shown in Figure 3c, was observed on an Ir(111) surface when it was annealed at ca. 1000 °C in a hydrogen−air flame. No atomically flat terraces can be seen in the image. This result indicates that the annealing temperature is one of the important factors to be controlled in exposing well-defined surfaces.

Finally, it is worthwhile to note that the atomically flat surface as shown in Figure 3a became rough, forming a rolling hill structure after several potential cycles between 0.05 and 1.5 V in either $HClO_4$ or H_2SO_4 solution. Such a surface roughening has been observed on Pt(111), Pd(111), and Rh(111) as described in our previous papers.[30−32]

In Situ STM in H_2SO_4. According to the CV shown in Figure 2, it is reasonable to expect that sulfate ions are strongly adsorbed on Ir(111). High-resolution STM imaging carried out on atomically flat terraces at 0.5 V in 0.1 M H_2SO_4 revealed atomic features in a relatively large area as shown in Figure 4a. It can be clearly seen that there are three domains rotated by 60° or 120°. The same atomic feature is seen in each domain. A careful observation revealed that the atomic rows are always along the [121] direction, showing 30° rotation with respect to the direction of the atomic rows of underlying Ir(111) lattice. Figure 4b presents another STM image acquired in an area of 15 × 15 nm in the image of Figure 4a. It can be seen that there are dark spots between neighboring bright rows. The observed features on Ir(111) shown in Figure 4a,b are very similar to those for the adsorbed sulfate on Au(111), Pt(111), Rh(111), and Cu(111).[8−15] Note that the images shown in Figures 4a and 4b reveal a distortion due to thermal drift.

Further details of the adlayer are revealed in Figure 4c, which is an atomic-resolution STM image acquired in a single sulfate domain. The acquisition of this image was performed specifically under conditions with minimal thermal drift in the *x* and *y* directions in order to determine the unit cell of the adlayer as accurately as possible. It can be seen that there are two different parallel rows along the [121] direction. One consists of bright spots and another dark spots. The observed average atomic distance in the bright rows along the A direction is ca. 0.47 nm ($\sqrt{3}\,a_{Ir}$). The average atomic distance along the B direction is ca. 0.71 nm ($\sqrt{7}\,a_{Ir}$). The angle between the atomic rows marked by arrows A and B is ca. 71°. From the orientation of atomic rows and the interatomic distances, we conclude that the sulfate adlayer on Ir(111) has the so-called ($\sqrt{3} \times \sqrt{7}$) structure as indicated by the unit cell marked in Figure 4c. The same structure was consistently observed in the potential range between 0.2 and 1.0 V.

For the sulfate adlayer on Rh(111), we previously proposed a structural model, in which chains of hydrogen-bonded water molecules are aligned along the $\sqrt{3}$ direction between neighboring rows of adsorbed sulfate species.[12] Bright and dark spots appearing in the STM images, respectively, were assumed to arise from the adsorbed sulfates and water molecules in the second layer of the first water bilayer. Identical structural models are proposed for the sulfate adlayer on Ir(111) surface. Figure 5a is an illustrative depiction of the adlayer structure, which is exactly the same as that proposed in our previous paper.[12] As pointed out in that paper, it is also possible to insert a hydrogen-bonded water chain with reversed configuration as shown in Figure 5b. In this case, the dark spots should appear almost at the center of the unit cell. Both configurations were found in our previous study on Rh(111).[12] Figure 5c shows the side view of a hydrogen-bonded water chain along the $\sqrt{3}$ direction.

Nevertheless, each chain of water molecules should appear in a zigzag configuration with different corrugation heights according to the model structures shown in Figure 5. However, only a single dark spot in the unit cell has been distinguished in previous studies using Au(111), Pt(111), Rh(111), and electrodes but not Cu(111) as described above.[8−15]

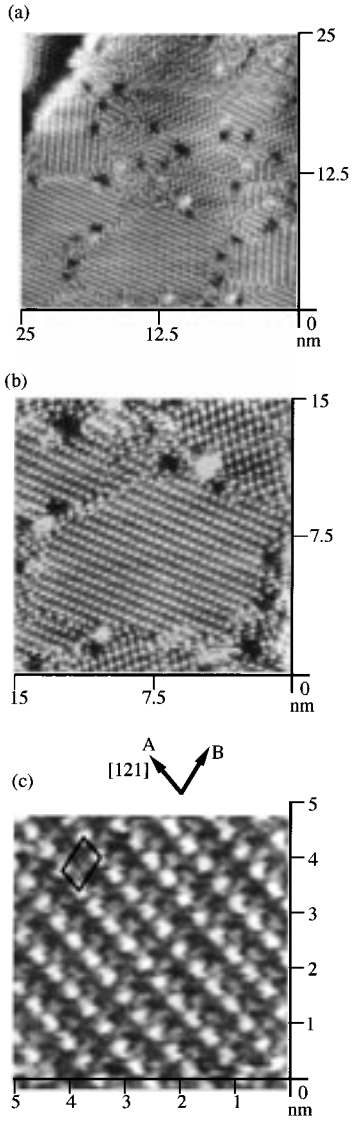

Figure 4. (a) In situ STM image of sulfate adlayers on Ir(111) surface in 0.1 M H_2SO_4 at 0.5 V. Scan area, 25 × 25 nm; tunneling current, 10 nA; tip potential, 0.4 V. (b) Close-up view of the lower portion of (a) acquired at a tunneling current of 5 nA. (c) STM image acquired in a single domain. A unit cell with ($\sqrt{3} \times \sqrt{7}$) symmetry is indicated. Tunneling current, 2 nA; tip potential, 0.4 V.

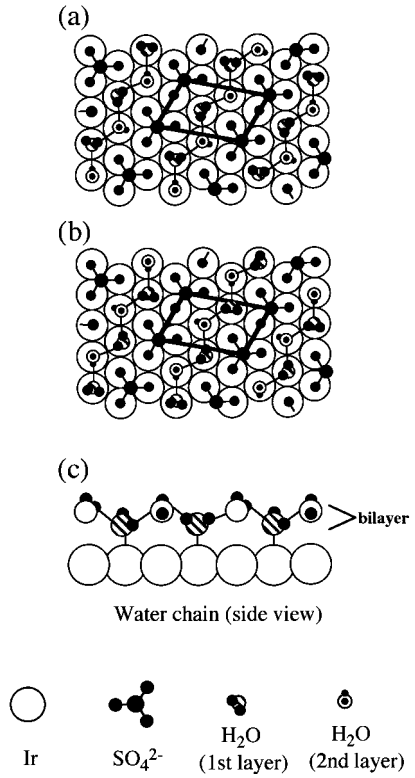

Figure 5. Illustrative depictions of the adlayer structure of Ir(111)−($\sqrt{3} \times \sqrt{7}$) sulfate, showing coadsorption of sulfate and hydrogen-bonded water chains. Two possible arrangements of water chains between two sulfate rows are illustrated by the models (a) and (b).

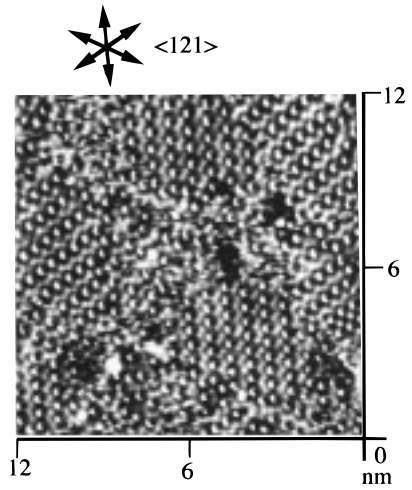

Figure 6. Unfiltered high-resolution STM image of sulfate adlayer on Ir(111) acquired at 0.5 V. Tunneling current, 20 nA; tip potential, 0.55 V. A zigzag row of hydrogen-bonded water is clearly seen between two sulfate rows. The arrows indicate the $\sqrt{3}$ direction of the underlying Ir(111) lattice.

Therefore, we paid our special attention to the dark spots seen in Figure 4c. To reveal details of the hydrogen-bonded water molecule, high-resolution STM images were acquired under carefully adjusted experimental conditions with minimal thermal drift. Surprisingly, a zigzag row of adsorbed hydrogen-bonded water molecules was clearly seen between two bright sulfate rows. Figure 6 is a typical unfiltered high-resolution STM image acquired in a relatively large area of 12 × 12 nm. This image was acquired at 0.5 V in 0.1 M H_2SO_4 at a tunneling current of 20 nA. The electrode potential of the tip was set at 0.55 V. Even in such a relatively large area, it can be seen clearly

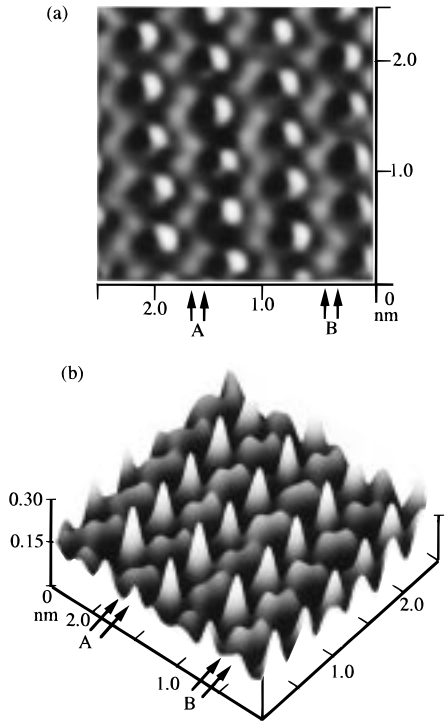

Figure 7. (a) Closeup top view in an area of Figure 6. (b) Height-shaded surface plot of (a). Both images were obtained by applying a mild two-dimensional Fourier transform filter method.

that almost all of the dark rows are composed of two separated spots in the unit cell, resulting in the formation of zigzag rows. It is also important to note that the dark spots with different corrugation heights are aligned alternately in the dark rows. The difference in corrugation height between the two dark spots was measured to be ca. 0.015−0.025 nm. This observation seems to be consistent with the models shown in Figure 5.

On the basis of the result described above, we strongly believe that the zigzag rows result from the existence of the hydrogen-bonded water chain. The water molecules in the second layer of the bilayer appear to be brighter than those in the first water layer.

Figure 7a shows a close-up image of one of the domains shown in Figure 6. The internal structure can be more clearly seen in the height-shaded surface plot shown in Figure 7b. We focused our attention on two sets of arrows marked A and B. The two arrows in each set indicate two sides of the corresponding zigzag water chain. It is clearly seen that the spots on the right-hand side of the chain marked A are higher in corrugation height than those on the left. On the other hand, the situation is reversed in the row marked B. This difference in the orientation of water molecules can be explained by the model structures shown in Figure 5a,b. The zigzag rows marked A result from the arrangement of water molecules illustrated in Figure 5a, because the brighter spots corresponding to the water molecules in the second layer appear along the right arrow in A. However, the brighter spots appear along the left arrow in B. This arrangement can be explained by the model shown in Figure 5b. It is clear that there are two different arrangements of water molecules in the adlayer of sulfate on Ir(111).

Finally, it is expected that high-resolution STM measurements can discriminate two different water molecules existing between the rows of adsorbed sulfate on (111) surfaces of other fcc metals such as Au, Pt, and Rh, which have previously been investigated using in situ STM.

Conclusions

Atomically flat Ir(111) surface with well-defined step-terrace structure was prepared using a flame-annealing−quenching technique. In $HClO_4$ solution, the Ir(111) showed a hexagonal structure with the atomic distance of 0.27 nm in the potential range from 0.1 to 1.0 V, indicating an unreconstructed (1×1) surface. Sulfate anions on Ir(111) in 0.1 M H_2SO_4 formed a highly ordered array with a $(\sqrt{3} \times \sqrt{7})$ symmetry with zigzag chains along the $\sqrt{3}$ direction between neighboring sulfate rows. The structural features observed in the STM images in the present study are consistent with those on Au(111), Pt(111), Rh(111), and Cu(111). A model for the coadsorption of water and sulfate was used to explain the observed adlayer structure. Higher resolution STM imaging revealed, for the first time, the structure of water molecules in both first and second layers of a bilayer. The height difference in the two layers was clearly observed.

Acknowledgment. This work was supported by a Grant-in-Aid for Science Research on Priority Area of "Electrochemistry of Ordered Interfaces" (No. 09237101) from the Ministry of Education, Science, Sports and Culture, Japan. The authors thank Dr. Y. Okinaka for his help in writing this manuscript.

References and Notes

(1) Gewirth, A. A.; Niece, B. K. *Chem. Rev.* **1997**, *97*, 1129.
(2) Itaya, K. *Prog. Surf. Sci.* **1998**, *58*, 121.
(3) Clavilier, J.; Faure, R.; Guinet, G.; Durand, R. *J. Electroanal. Chem.* **1980**, *107*, 205.
(4) Clavilier, J. *J. Electroanal. Chem.* **1980**, *107*, 205.
(5) Clavilier, J.; Rodes, A.; Achi, K. El.; Zamakhchari, M. A. *J. Chim. Phys.* **1991**, *88*, 1291.
(6) Furuya, N.; Kiode, S. *Surf. Sci.* **1989**, *220*, 18.
(7) Feliu, J. M.; Orts, J. M.; Gomez, R.; Aldaz, A.; Clavilier, J. *J. Electroanal. Chem.* **1994**, *372*, 265.
(8) Magnussen, O. M.; Hagebock, J.; Hotlos, J.; Behm, R. J. *Faraday Discuss.* **1992**, *94*, 329.
(9) Edens, G. J.; Gao, X.; Weaver, M. J. *J. Electroanal. Chem.* **1994**, *375*, 357.
(10) Funtikov, A. M.; Linke, U.; Stimming, U.; Vogel, A. *Surf. Sci. Lett.* **1995**, *324*, L343.
(11) Funtikov, A. M.; Stimming, U.; Vogel, A. *J. Electroanal. Chem.* **1997**, *428*, 147.
(12) Wan, L.-J.; Yau, S.-L.; Itaya, K. *J. Phys. Chem.* **1995**, *99*, 9507.
(13) Wilms, M.; Broekmann, P.; Kruft, M.; Park, Z.; Stuhlmann, C.; Wandelt, K. *Surf. Sci.* **1998**, *83*−*86*, 402.
(14) Wilms, M.; Broekmann, P.; Stuhlmann, C.; Wandelt, K. *Surf. Sci.* **1998**, *416*, 121.
(15) Li, W.; Nichols, R. J. *J. Electroanal. Chem.* **1998**, *456*, 153.
(16) Shi, Z.; Lipkowski, J.; Gamboa, M.; Zelenay, P.; Wieckowski, A. *J. Electroanal. Chem.* **1994**, *366*, 317.
(17) Hourani, M.; Wasberg, M.; Rhee, C. K.; Wieckowski, A. *Croat. Chem. Acta* **1990**, *63*, 373.
(18) Wasberg, M.; Hourani, M.; Wieckowski, A. *J. Electroanal. Chem.* **1990**, *278*, 425.
(19) Zelenay, P.; Horanyi, G.; Rhee, C. K.; Wieckowski, A. *J. Electroanal. Chem.* **1991**, *300*, 499.
(20) Zelenay, P.; Wieckowski, A. *J. Electrochem. Soc.* **1992**, *139*, 2552.
(21) Motoo, S.; Furuya, N. *J. Electroanal. Chem.* **1984**, *167*, 309.
(22) Motoo, S.; Furuya, N. *J. Electroanal. Chem.* **1984**, *181*, 301.
(23) Motoo, S.; Furuya, N. *J. Electroanal. Chem.* **1986**, *197*, 209.
(24) Jiang, X.; Chang, S.-C.; Weaver, M. J. *J. Phys. Chem.* **1991**, *95*, 7453.
(25) Gomez, R.; Weaver, M. J. *J. Electroanal. Chem.* **1997**, *435*, 206.
(26) Gomez, R.; Weaver, M. J. *Langmuir* **1998**, *14*, 2525.
(27) Gomez, R.; Weaver, M. J. *J. Phys. Chem. B* **1998**, *102*, 3754.
(28) Tang, C.; Zou, S.; Severson, M. W.; Weaver, M. J. *J. Phys. Chem. B* **1998**, *102*, 8546.
(29) Hoshi, N.; Uchida, T.; Mizumura, T.; Hori, Y. *J. Electroanal. Chem.* **1995**, *381*, 261.
(30) Itaya, K.; Sugawara, S.; Sashikata, K.; Furuya, N. *J. Vac. Sci. Technol.* **1990**, *A8*, 515.
(31) Sashikata, K.; N. Furuya, N.; Itaya, K. *J. Vac. Sci. Technol.* **1991**, *B9*, 457.
(32) Wan, L.-J.; Yau, S.-L.; Swain G. M.; Itaya, K. *J. Electroanal. Chem.* **1995**, *381*, 105.